**ORIGINAL PAPER**

# Time-resolved pressure-sensitive paint measurements for cryogenic wind tunnel tests

Daisuke Yorita[1] · Ulrich Henne[1] · Christian Klein[1]

## Abstract

A first time-resolved pressure-sensitive paint (PSP) test campaign at the European Transonic Wind Tunnel (ETW) was conducted within the research initiative "Unsteady flow and interaction phenomena at High Speed Stall conditions". One of the objectives of this wind tunnel campaign was to resolve time-series of surface pressure distributions caused by complex 3-D buffet phenomena on a full-span airplane model XRF-1 transport aircraft configuration. At higher angle-of-attack and high Mach number, pressure fluctuations with a frequency of several hundred Hertz are expected to occur on the main wing and the horizontal tail plane (HTP) caused by the buffet effect. To capture the expected buffet phenomena by PSP, the German Aerospace Center developed a time-resolved PSP measurement and data acquisition system as well as a post-processing method for measurements in ETW. The measurements were conducted on the main wing and HTP simultaneously, with a camera frame rate of up to 2 kHz. The transonic buffet phenomena were observed at the flight relevant Reynolds number $Re = 12.9 \times 10^6$ and $Re = 25.0 \times 10^6$. The time-varying surface pressure distribution on the model was successfully captured by PSP. The time-series and spectra of both PSP and pressure transducer data match very well.

**Keywords** Pressure-sensitive paint · Cryogenic · Time-resolved measurement · Transonic buffet

## 1 Introduction

Pressure-sensitive paint (PSP) is an optical pressure measurement technique which is based on oxygen quenching and which is widely used in wind tunnel testing [1]. A great advantage of the PSP technique is that a surface pressure distribution over a model can be obtained quantitatively with high spatial resolution. Nowadays, time-resolved PSP measurement with acquisition frequencies of several kilohertz is possible and has been reported in various applications [2–4].

However, it is not straightforward to apply the PSP technique to cryogenic wind tunnel testing. A cryogenic test aims to achieve those high Reynolds number conditions in ground facilities that pertain to aircraft flight. The cryogenic

tests require high-pressure and low-temperature conditions and this is quite different compared to those encountered in non-cryogenic wind tunnels. The European Transonic Wind-tunnel (ETW) is one of the largest cryogenic wind tunnels in the world [5]. ETW is operated with cold nitrogen as a test gas to decrease the temperature down to 110 K and can be pressurized up to 450 kPa. The German Aerospace Center (DLR), the University of Hohenheim and ETW have further developed the PSP technique to be applicable to cryogenic wind tunnel testing [6–8]. PSP measurement in ETW can provide high-quality pressure data, but so far its capability has been limited to time-averaged (mean) pressure data.

The first time-resolved PSP measurement in ETW was conducted within the research initiative "Unsteady flow and interaction phenomena at High Speed Stall conditions" [9]. One of the objectives of this wind tunnel campaign was to resolve time-series of surface pressure distributions caused by complex 3-D buffet phenomena on a full model XRF-1 transport aircraft configuration [10]. A picture of the XRF-1 model is shown in Fig. 1. At higher angle-of-attack and high Mach number, pressure fluctuations with a frequency of several hundred Hertz are expected to occur on the main wing and horizontal tail plane (HTP); these are caused by the

✉ Daisuke Yorita
daisuke.yorita@dlr.de

Ulrich Henne
ulrich.henne@dlr.de

Christian Klein
christian.klein@dlr.de

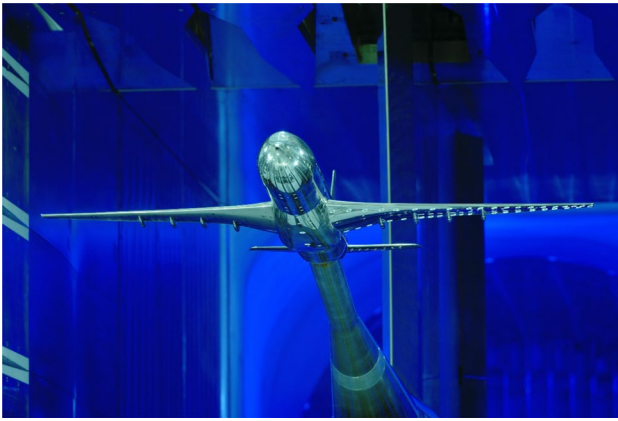1 German Aerospace Center (DLR), Bunsenstrasse 10, 37073 Göttingen, Germany

**Fig. 1** XRF-1 model in the ETW test section

buffet effect. To capture the expected buffet phenomena by PSP, DLR developed a time-resolved PSP measurement and data acquisition system as well as a post-processing method for measurements in ETW. This work gives an overview of the time-resolved PSP measurements for tests in ETW at cryogenic conditions.

## 2 Pressure-sensitive paint techniques for cryogenic tests

### 2.1 Principle

Pressure measurements by means of PSP are based on the photo-physical phenomenon of luminophores known as oxygen quenching, where the intensity and lifetime of photoluminescence are reduced due to quenching by the presence of oxygen molecules: specifically, higher concentrations of oxygen result in reduced intensity and shorter lifetime of photoluminescence, while lower oxygen concentrations result in increased intensity and longer lifetime [1]. According to Henry's law, the concentration of oxygen in the PSP layer is proportional to the partial pressure of oxygen of the gas above the surface. Therefore, if the oxygen concentration in the gas is constant, pressure can be related to the photoluminescent intensity and lifetime of the PSP luminophore. The method actually measures oxygen (or gas) density/concentration, but with a knowledge of the gas temperature and appropriate calibration, pressure values can then be obtained.

### 2.2 Time-resolved PSP measurement in ETW

The ETW is one of the largest cryogenic wind tunnels in the world. ETW is operated with cold nitrogen as a test gas to decrease the temperature down to 110 K and can be pressurized up to 450 kPa. With these low temperature and

high pressure conditions, Reynolds numbers relevant for aircraft flight can be achieved. A small concentration of oxygen (approximately 1000 ppm) is added to the nitrogen test gas during the PSP measurement.

The existing PSP technique in ETW is the two-gate lifetime method for steady (or time-averaged) pressure measurements [7, 11]. In the two-gate method, two luminescent images are acquired at different timing of the pulsed excitation and the luminescence decay (so-called Gate1 and Gate2 image). Therefore, the two-gate lifetime system requires a pulsed excitation light source and a fast-shutter (and usually multi-exposure) camera. A reason for use of this method is to overcome problems arising from large model deformation or displacement during the wind tunnel test. Due to the high aerodynamic load on the model, the model shape and position are changed between the test (wind-on) and the static (wind-off) conditions. This introduces a critical measurement error when using the intensity PSP method, whereas the lifetime method is not susceptible to errors caused by model deformation or displacement. However, a typical data acquisition rate of the steady PSP system in ETW is limited to 1 Hz or slower, so that it is not possible to resolve the buffet pressure fluctuations occurring at frequencies of several hundred hertz.

For the time-resolved PSP measurement in ETW, only with the intensity PSP method it is possible to achieve PSP data acquisition rates above 1 kHz. In the intensity method, the high-speed camera can be used with constant excitation light. The intensity method requires images to be taken during wind-on and reference (normally wind-off) conditions, but then model deformation or displacement problems crop up. Instead of using the wind-off PSP image as reference, it is known that a time-averaged (mean) wind-on PSP image can be used as the reference image [12]. In this case, a pressure ratio rather than an absolute pressure is obtained:

$$P_i/P_{\mathrm{mean}} = a \cdot I_{\mathrm{mean}}/I_i, \tag{1}$$

where $a$, $I$ and $P$ are a pressure calibration factor, PSP intensity and pressure, respectively. The subscripts $i$ and mean represent an image index and time-averaged data. This method is especially effective for applications to low-speed flows and acoustics fields, where the mean pressure is almost constant over the surface. However, for application in the high-speed test in ETW, information of the mean pressure is required to obtain absolute pressure because the mean pressure field contains large pressure variations.

Therefore, it was decided that both 'steady' lifetime PSP and 'unsteady' intensity PSP measurements are necessary in this test. The mean pressure information is measured by the steady PSP measurement and the pressure variation information is from the unsteady PSP measurement. Then, in the post-processing, the time-resolved absolute

pressure is reconstructed from two PSP measurements using Eq. (2):

$$P_i = \left(P_{\text{mean}}\right)_{\text{steady}} \cdot \left(P_i/P_{\text{mean}}\right)_{\text{unsteady}}. \tag{2}$$

## 2.3 Paint

The paint for the PSP measurements requires high pressure sensitivity and fast response time under cryogenic conditions. The luminescence dye used in this test is composed of the luminophore platinum-mesotetra(pentafluorophenyl) porphine (PtTFPP) [13] and the binder poly(trimethylsily) propyne (poly(TMSP)) [14]. PtTFPP has an acceptably fast lifetime decay time (50 µs under vacuum condition) and a high luminescent intensity. Poly(TMSP) is known to have the highest oxygen permeability amongst known polymers. This very high oxygen permeability provides high pressure sensitivity at the cryogenic condition and a fast response time for the time-resolved PSP measurements. Further information of the paint characteristics can be found in references [6, 7], and a demonstration of the paint response for pressure fluctuations above 100 Hz is introduced in reference [15].

A summary of the time-resolved PSP measurements in ETW is shown in Table 1.

## 3 Experimental setup

## 3.1 PSP coating

The PSP coating was applied after finishing all other model preparations. The areas where the PSP coating has not been applied (viz., the pressure sensors and the flap track fairings) were covered by a masking tape. After careful cleaning of the model surface by Acetone, 3-D target markers were applied on the model metal surface using a black pen. The screw holes filled with filler material were also masked using a black pen since the filler material used in this test interacted with the PSP paint. After these preparations, the PSP coating was directly sprayed onto the model surface without a primer or basecoat layer, to avoid any interactions between the layers. This enabled the application of the PSP coating

**Table 1** Summary of the time-resolved PSP measurements in ETW

| Measurement | Steady PSP | Unsteady PSP |
|---|---|---|
| PSP method | Lifetime | Intensity |
| Pressure data | Mean (time-averaged) | Variation (amplitude) |
| Camera | Multi-exposure camera | High-speed camera |
| Excitation light | Pulsed | Constant |
| Paint | PtTFPP / poly(TMSP) | |

to be the final procedure of the model preparation, reducing the risk of unexpected contacts and contamination of the coating surface. The thickness of the paint was below 5 µm. The roughness of the paint was approximately 0.15–0.3 µm in the arithmetic average roughness $R_a$ [7].

## 3.2 Equipment and installation

### 3.2.1 Steady PSP system

A UV-LED unit developed by ETW and ILA GmbH for cryogenic wind tunnel tests was used. Four LED chips with a 405 nm peak wavelength can be externally operated in pulsed mode for the lifetime PSP method. The LED head and control electronics were designed to fit into a heated cylindrical temperature-protection housing to protect the equipment from cold nitrogen gas. A $385 \pm 35$ nm optical band-pass filter was attached in front of the LEDs. Additionally, a cylindrical lens and a diffusion foil were installed in front of the optical filter to improve the illumination distribution on the model surface.

A CCD camera (PCO4000, PCO) with a $650 \pm 50$ nm optical band-pass filter was installed in a separate temperature-protection housing. This camera has a capability of "modulation mode", which enables the multi-exposure accumulation on the sensor chip using an external control signal [11]. The lens was equipped with remote focus and aperture controls to adjust for the large model position changes during the test. A manual mechanical tilt mechanism ($\pm 10$ degrees) was also installed to adjust the camera angle inside the housing.

### 3.2.2 Unsteady PSP system

The same LED unit used for the steady PSP system can be used for the unsteady PSP system with a constant illumination mode for the intensity PSP method.

A high-speed CMOS camera, FASTCAM Mini AX 200 (Photron), was used for the tests. The camera was equipped with the same type of optical filter as the steady PSP system. The camera has 32 GB memory on board, enabling storage of 21,840 images with full image resolution. The image readout time for the full camera memory was approximately 5 min in this test.

### 3.2.3 Optical configuration

All PSP systems were installed on the wind tunnel floor. The model wing and HTP surfaces were separately observed by two sets of PSP systems. One steady camera, one high-speed camera and two LEDs were used for the model wing view while one LED was used for the model HTP view. The

model upper and lower surfaces were measured by rotating the model by 180 degrees.

## 3.3 Data acquisition

Since the steady and the unsteady PSP measurements operated with the same LED unit but in different operation modes, the two PSP measurements needed to be conducted separately. In order to reduce nitrogen consumption during the PSP test campaign, the sequence and priority of the PSP data acquisition was carefully selected to minimize the wind tunnel operation time. A large nitrogen consumption occurred during stop and start of the wind tunnel. Therefore, the sequence and priority (SP) of the PSP data acquisition were set as follows:

SP1: Angle-of-attack change.
SP2: Mach number change.
SP3: Switching between the steady and the unsteady PSP system.
SP4: Model orientation change by 180 degrees.

### 3.3.1 Steady PSP system

The steady PSP system can be operated with a parallel image acquisition and image readout. Five gated PSP images (3 Gate1 and 2 Gate2) were alternately acquired at one data point. The image acquisition timing of the wing and the HTP view were synchronized by an external trigger. The data acquisition SP1 and SP2 could be set into one data block without stopping the wind tunnel. For a reliable operation of the steady PSP system, the procedure of the data acquisition was fully automated during the tunnel operation. In the future test campaigns, duration of SP3 can be minimized and the wind tunnel stop will not be required at SP3. Due to tunnel operation limitations, the wind tunnel stop at SP4 is always necessary.

### 3.3.2 Unsteady PSP system

The unsteady PSP system has an additional limitation from the camera memory size. The high-speed camera can store up to 21,840 images in its memory, where approximately 5 min readout time was required. During this camera image readout, the wind tunnel needed to be stopped to reduce the nitrogen consumption. The camera can split the memory into multiple partitions. In this test, 4, 5 or 6 memory partitions were used, resulting in 5460, 4368 or 3640 images to be acquired at one data point, respectively. The image frame rate depended on the test conditions. A sampling rate of 2 kHz could be achieved for tests conducted at temperatures of 180 K ($Re = 12.9$ million) while 1 kHz sampling rate was used at 115 K ($Re = 25.0$ million) because of lower PSP light

intensity at lower temperature. The image acquisition timing of the wing and the HTP view were synchronized by an external trigger. The timing of the high-speed camera acquisition was recorded in the ETW high-speed data acquisition system which also records the unsteady pressure transducer signals. Therefore, a direct comparison of the time-resolved PSP data and the unsteady pressure transducer data is possible in the post-processing.

## 3.4 Pressure calibration

An in situ pressure calibration was necessary for both the steady and the unsteady PSP data, because the oxygen concentration in the wind tunnel changed slightly during the test.

### 3.4.1 Steady PSP data

The in situ calibration of the steady PSP data was done with the static pressure tap data. The calibration coefficients were calculated from the relation between the ratio-of-ratios PSP data and the static pressure data, as shown in Fig. 2. Further information is summarized in reference [8].

### 3.4.2 Unsteady PSP data

The in situ calibration of the unsteady PSP data was done by using the unsteady pressure transducer data which were measured synchronously. As mentioned in the Sect. 2, the unsteady PSP system can capture only the variations of pressure ratio $P/P_{mean}$, which is calculated from the ratio of the mean (time-averaged) PSP intensity and the temporal PSP intensity $I_{mean}/I$. Based on Eq. (1), the calibration coefficient was calculated as the ratio of the standard deviations of pressure ratio and PSP intensity ratio (see Fig. 3). It is desirable to calculate a calibration factor at each data point, but this was difficult, because the pressure fluctuations did not always appear near a pressure transducer location. Therefore, the same calibration coefficient was used for all data points at one flow condition.
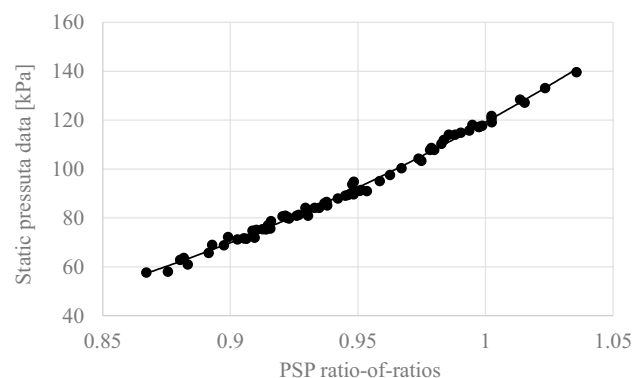


**Fig. 2** Example of the in situ calibration for the steady PSP data
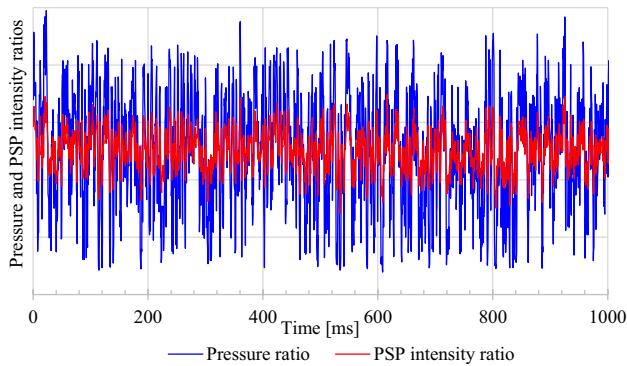
**Fig. 3** The comparison between the pressure ratio and the PSP intensity ratio. The ratio of the standard deviations is used as the calibration coefficient
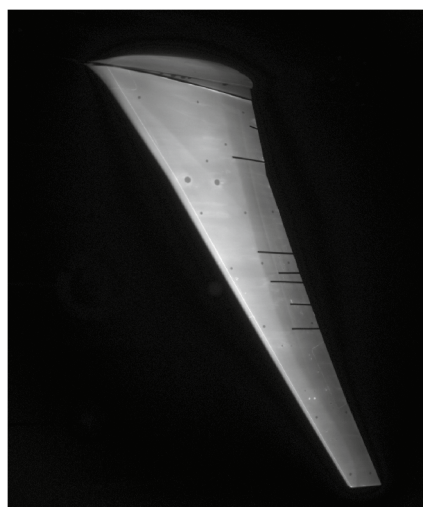
### 3.4.3 Time-resolved absolute pressure data

After the pressure calibrations, the time-resolved absolute pressure was reconstructed by the superposition of the steady PSP data and the unsteady PSP data. Both PSP data were mapped on the same 3-D grid and multiplied based on Eq. (2).
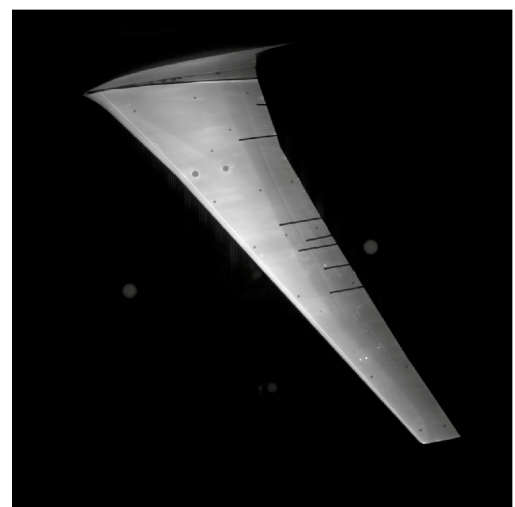
## 4 Results and discussion

### 4.1 Overview of PSP data

Raw intensity (grayscale) steady and unsteady PSP images are shown in Fig. 4. All PSP images shown in this subsection were acquired at flow conditions of $Re = 12.9$ million, $M = 0.84$ and $\alpha = +4$ degrees. The steady and unsteady PSP cameras have different viewing angles of the model surface. These PSP images were mapped on the same 3-D grid

surface to apply the post-processing in the same coordinate system. In both raw PSP images, the shock position was clearly visible as a high-to-low PSP intensity step. The black lines near the trailing edge corresponded to the unsteady pressure transducer rows where the PSP coating had not been applied. A thin, white line downstream of the shock is an optical error caused by the shock.

The steady PSP data calculated to the mean pressure is shown in Fig. 5. The mean pressure distribution over the wing can be obtained after removing or suppressing most of the artificial patterns, including the afore-mentioned shock optical error line. The three consecutive unsteady PSP images calculated to the pressure variation are shown in Fig. 6. The pressure variation from the wing mid part to the outer part was well captured. In the unsteady PSP data, the shock optical error line was still visible: this is because the magnitude and position of this artefact was different for images at each unsteady PSP snapshot and at the time-averaged unsteady reference PSP.
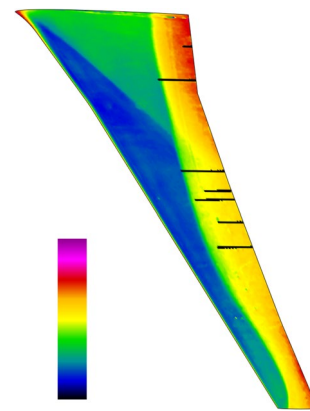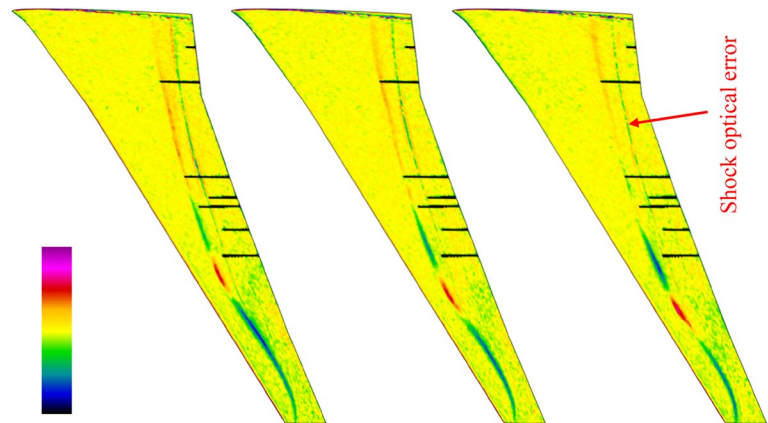


**Fig. 5** The steady PSP data calculated to the mean pressure

**Fig. 4** The raw intensity (grayscale) PSP images



(a) Steady PSP camera

(b) Unsteady PSP camera

**Fig. 6** Three-consecutive unsteady PSP images calculated relative to the pressure variation ($\Delta t = 0.5$ ms)

The absolute time-resolved PSP data obtained by the superposition of the steady and the unsteady PSP data are shown in Fig. 7. The shock shape at the outer wing of the time-resolved PSP data was complexly curved compared to that of the steady PSP data. The pressure patterns seem to be traveling from the wing inner part to the outer part, which has been typically explained as a spanwise propagation of the buffet cells. The comparisons between the time-resolved PSP data and the pressure transducer data in time and in frequency are shown in Fig. 8 (Point A in Fig. 7). The amplitudes and spectra of both data match very well. One of the great advantages of the PSP data is that the pressure information can be obtained for any arbitrary point on the surface. Figure 9 shows the time-resolved PSP data in time and in frequency at the wing outer part where the strong pressure fluctuation occurred (Point B in Fig. 7). Compared to the wing inner part, a higher frequency pressure fluctuation was observed with a broadband frequency around 200–600 Hz. The valuable time-resolved PSP data for understanding the complex 3-D buffet phenomena were obtained in the flight relevant Reynolds number conditions in this test.

## 4.2 Errors and technical problems

The errors, uncertainties and technical problems in the current time-resolved PSP measurements at cryogenic conditions are discussed in this part.

The dominant error of the time-resolved PSP data is the camera shot-noise. This noise appears randomly at image pixel-to-pixel and in time. It has been reported that the advanced image processing methods such as proper orthogonal decomposition (POD) and dynamic mode decomposition (DMD) are useful to reduce the shot-noise from the time-resolved PSP data [16, 17]. The pressure fluctuation expected in this test is a superposition of the strong pressure fluctuation by the buffet and the weak pressure fluctuation of the separated flow behind the shock. POD or DMD must be carefully applied to the time-resolved PSP data in order to avoid removal of weak pressure fluctuations.

Another problem is an optical error caused by the Schlieren effect. Due to the large density change by the shock, the excitation light and/or the emitted PSP light were refracted, consequently appearing as the stripe pattern error (artefact) in the PSP images. The pressure fluctuation distribution obtained by a root-mean-square (RMS) analysis is



**Fig. 7** Three-consecutive time-resolved PSP data obtained by the superposition of the steady and the unsteady PSP data
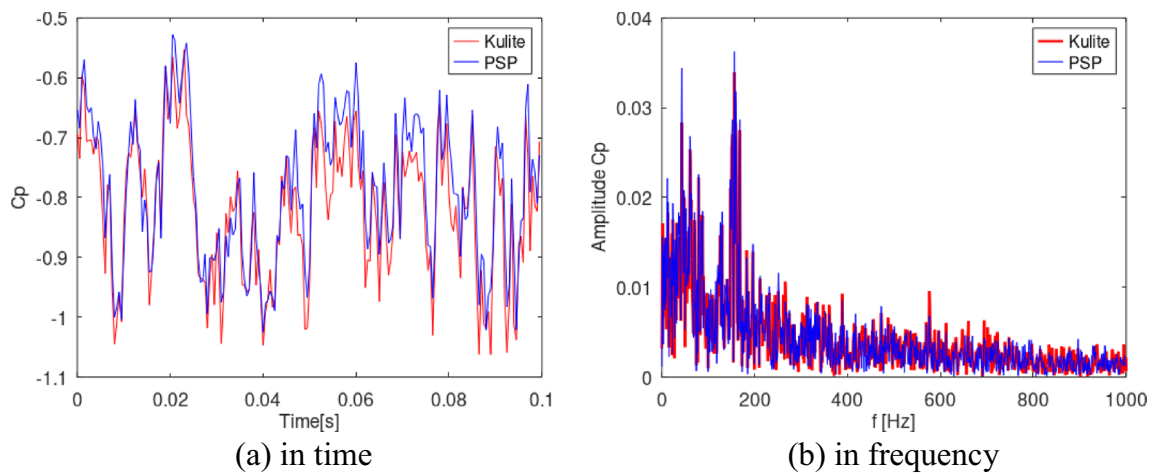
(a) in time    (b) in frequency
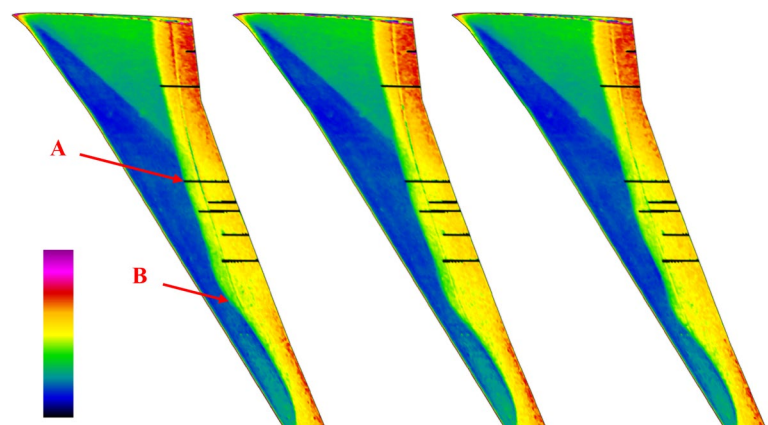
**Fig. 8** The comparisons between the time-resolved PSP data and the pressure transducer data at the position A in Fig. 7



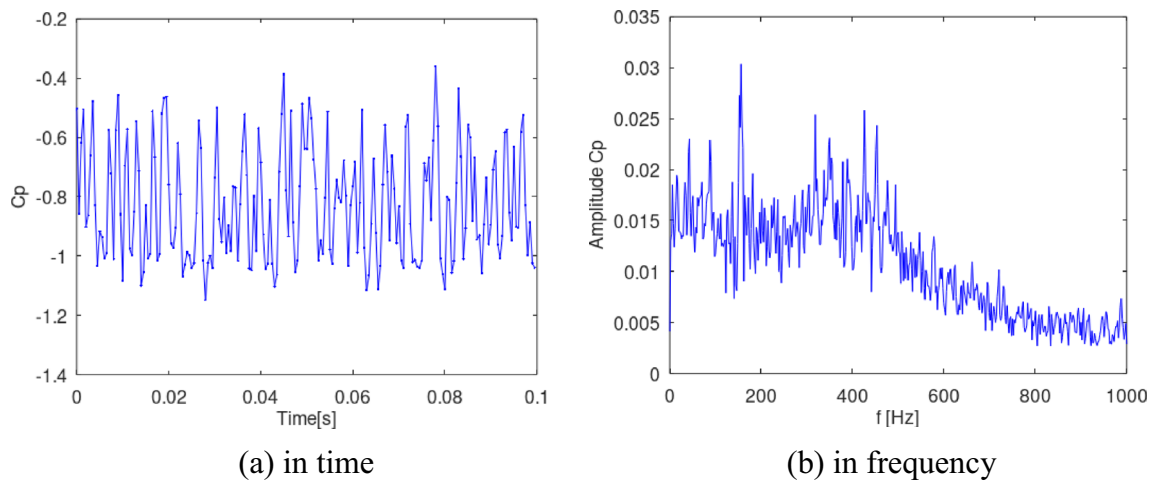(a) in time    (b) in frequency

**Fig. 9** The time-resolved PSP data in time (**a**) and frequency (**b**) at the position B in Fig. 7

shown in Fig. 10. Details of the RMS analysis of the PSP data is introduced in the Appendix. In the image, the front curved line is the pressure fluctuation area caused by the buffeting effect and the rear straight line is due to the optical artefact. The position of the optical error depends on many parameters, e.g., the positions of the LED and the camera, the model angle-of-attack and the shock location above the model. Therefore, it is very difficult to avoid this error with the present PSP optical setup for all PSP data acquired in a wide range of the angles-of-attack and flow conditions. It would need to be subtracted in the post-processing by using some effective method such as the above-mentioned POD or DMD.

The frequency response of the PSP paint needs to be carefully investigated. The pressure fluctuations in this test showed a broadband frequency range. The response of PSP might change with frequency. Thus, frequency or step
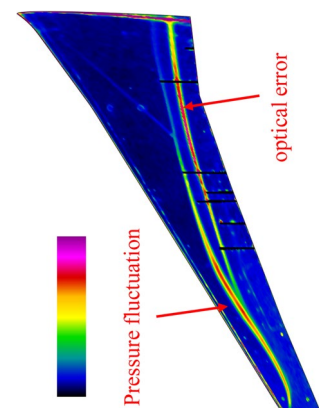


**Fig. 10** The pressure fluctuation map obtained by the RMS analysis of the PSP data

response tests would be required at cryogenic conditions to obtain a transfer function.

## 5 Conclusions

The first time-resolved PSP test campaign at the ETW was conducted within the research initiative "Unsteady flow and interaction phenomena at High Speed Stall conditions". This work represented the first time-resolved PSP measurement under cryogenic conditions in an industrial wind tunnel. The lifetime-based steady PSP measurement and the intensity-based unsteady PSP measurements were conducted on the wing and the HTP surfaces of the full-span airplane model XRF-1 to capture the pressure fluctuations caused by the complex 3-D buffeting phenomenon. The PSP system can capture the time-resolved pressure data with a sampling frequency up to 2 kHz depending on the test conditions. The PSP measurement system, the data acquisition and the data processing methods have been presented in great detail. The time-resolved absolute pressure can be reconstructed by the superposition of the steady PSP data and the unsteady PSP data. The obtained time-resolved PSP data successfully captured the quantitative pressure fluctuations caused by the buffeting effect. Both the time-series and spectra PSP data agreed well with the unsteady pressure transducer data. In future, advanced PSP data analysis like the POD and DMD will be applied to enhance the SNR of the PSP data and to remove the optical error caused by the shock.

## Appendix

## Noise reduction for root-mean-square analysis

A root-mean-square (RMS) analysis can visualize the pressure fluctuations on the model surface. A quantitative pressure amplitude comparison is also possible with a proper pressure calibration and a background noise subtraction.

The simple RMS analysis of the unsteady PSP data can be defined as in Eq. (3):

$$\left(\frac{P}{P_{\mathrm{mean}}}\right)_{\mathrm{RMS}} = a \cdot \left(\frac{I_{\mathrm{mean}}}{I}\right)_{\mathrm{RMS}} = a \cdot \sqrt{\frac{1}{N} \cdot \sum_{i=0}^{N} \left(\frac{I_{\mathrm{mean}}}{I_i} - 1\right)^2}$$

(3)

where $N$ is the number of PSP images. However, the variation of the PSP intensity is a superposition of both the pressure fluctuation and the shot-noise fluctuation from the camera.

$$\left(\frac{I_{\mathrm{mean}}}{I}\right)_{\mathrm{RMS}} = \sqrt{\sigma_P^2 + \sigma_{\mathrm{SN}}^2}$$

(4)

where the $\sigma_P$ and $\sigma_{\mathrm{SN}}$ are the intensity ratio variation caused by the pressure fluctuation and the camera shot-noise, respectively. Thus, the camera shot-noise appears as an offset error in the RMS PSP data. It is known that the standard deviation of the shot-noise in the intensity ratio PSP data is approximately proportional to an inverse of the square root of intensity [1]. In the general approach, this shot-noise offset error was often estimated using the wind-off PSP data, which has a similar PSP intensity distribution as the wind-on PSP data but without pressure fluctuation [18]. However, when the strong shock appears on the model surface, the PSP intensity between the wind-on and the wind-off data varies a lot and the simple estimation of the offset noise level from the wind-off PSP data does not work properly.

In this study, the camera calibration for the correction of the shot-noise offset error was employed. Here, the unsteady PSP intensity in the camera image was varied in the dynamic range of the camera and the time-series wind-off data was acquired at each intensity level. In ETW, the PSP intensity level can be varied by changing the LED power, the camera exposure time and the wind tunnel conditions (pressure, temperature and the oxygen concentration). Figure 11a shows a relation between the PSP intensity and the shot-noise RMS in the camera dynamic range. Figure 11b shows the same data but the x-axis is now the inverse of the square root of intensity. The relation is not perfectly linear due to other noise components but the function between the PSP intensity and the shot-noise RMS can be obtained over a wide intensity range. By using this function, the shot-noise offset RMS can be estimated quantitatively from the wind-on PSP intensity data.

One demonstration of the shot-noise RMS subtraction from the PSP RMS data is shown in here. Figure 12a is the wind-on PSP intensity distribution (mean) on the wing and Fig. 12b is the PSP RMS distribution including the shot-noise RMS. The wing view is plotted with orthogonal axes to help identify local pressure structures. The x-axis is the chord direction (the leading edge is left) and the y-axis is the span direction (the wing tip is bottom). In the PSP RMS data, three curved RMS lines along the span direction are visible. The first line from the leading edge is the high pressure RMS area due to the buffet shock oscillation, and the latter two lines are shock-induced optical errors. In other areas, there are trends that the RMS level is lower in front of the shock and higher behind the shock especially around the wing root and tip area. These are due to a superposition of the pressure fluctuations and the shot-noise. Figure 12c shows the shot-noise RMS distribution estimated from the wind-on PSP intensity distribution (Fig. 12a) by using the relation between the PSP intensity and the shot-noise RMS
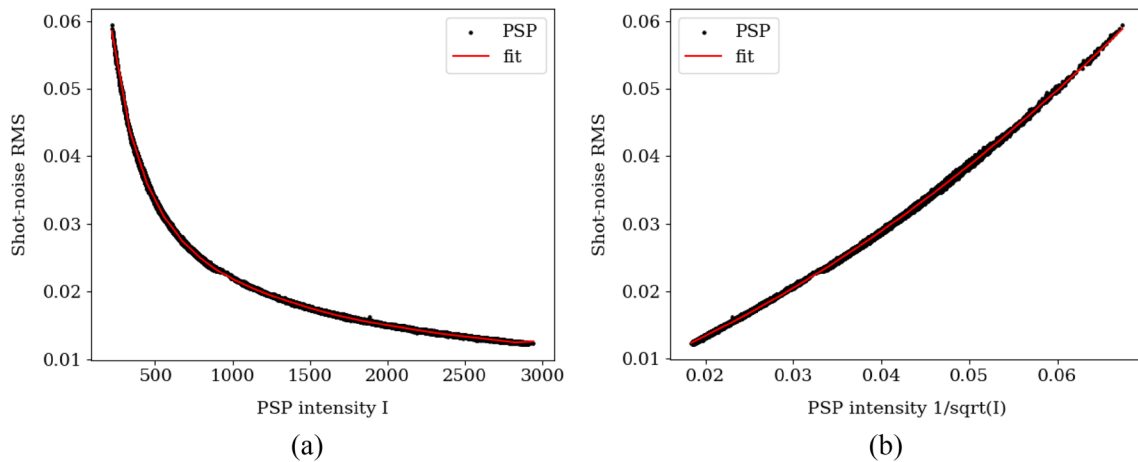
Fig. 11 The relation between the PSP intensity and the shot-noise RMS



(a) Wind-on PSP intensity  (b) Wind-on PSP RMS including shot-noise RMS  (c) Wind-on shot-noise RMS estimated from (a)  (d) Wind-on PSP RMS subtracted by (c)
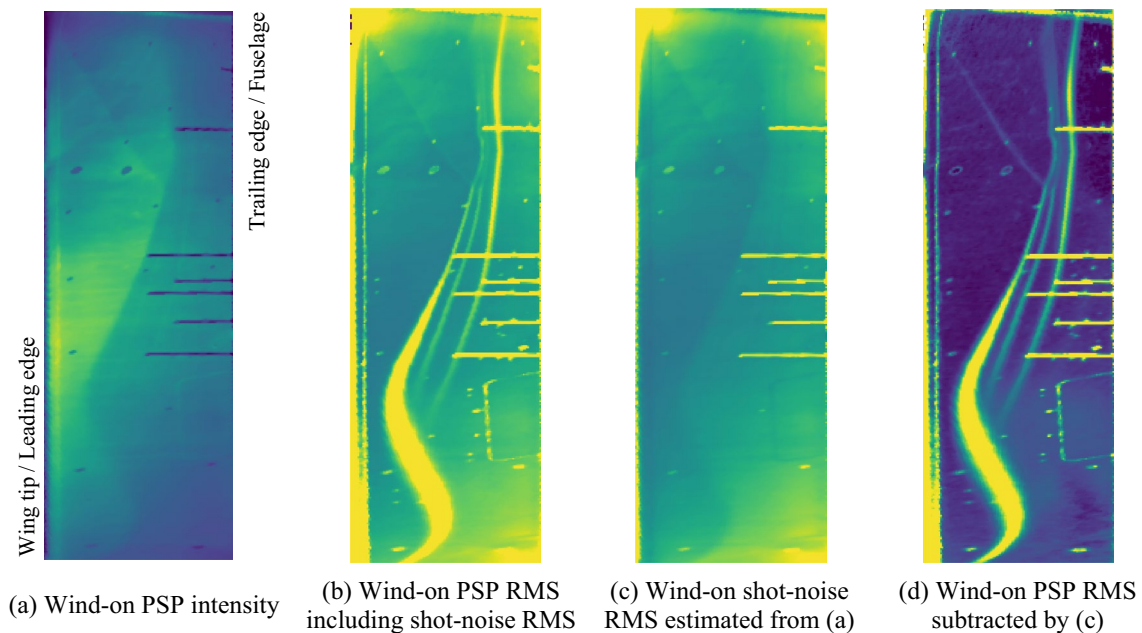
Fig. 12 Shot-noise RMS subtraction from the PSP RMS data by the proposed method

(Fig. 11). The estimated shot-noise RMS distribution represents quite well the wind-on PSP intensity distribution, with lower/higher RMS at higher/lower intensities, respectively.

Figure 12d shows the wind-on PSP RMS distribution with the shot-noise RMS subtraction applied. After the noise reduction, the RMS level at the areas in front and behind the shock are almost the same (nearly 0). Near the wing tip, the area behind the shock shows slightly higher RMS level. In this area, a flow separation is assumed behind the shock and thus small pressure fluctuations occurs. After the proper noise subtraction, such small pressure fluctuations can be distinguished in the PSP RMS data.

As mentioned above, it is common to use the wind-off PSP data for the shot-noise RMS subtraction. In Fig. 13a–d, the wind-off PSP intensity distribution, the wind-on PSP RMS distribution including the shot-noise RMS, the wind-off PSP RMS distribution and the wind-on PSP RMS distribution with the shot-noise RMS subtraction by wind-off PSP RMS are shown, respectively. Since the PSP intensities are different between the wind-on and wind-off PSP data, the shot-noise RMS is not correctly obtained. As a result, in the noise subtracted PSP data, the RMS level at the area in front of the shock shows values below 0 and the residual shot-noise error is superposed on the pressure fluctuation
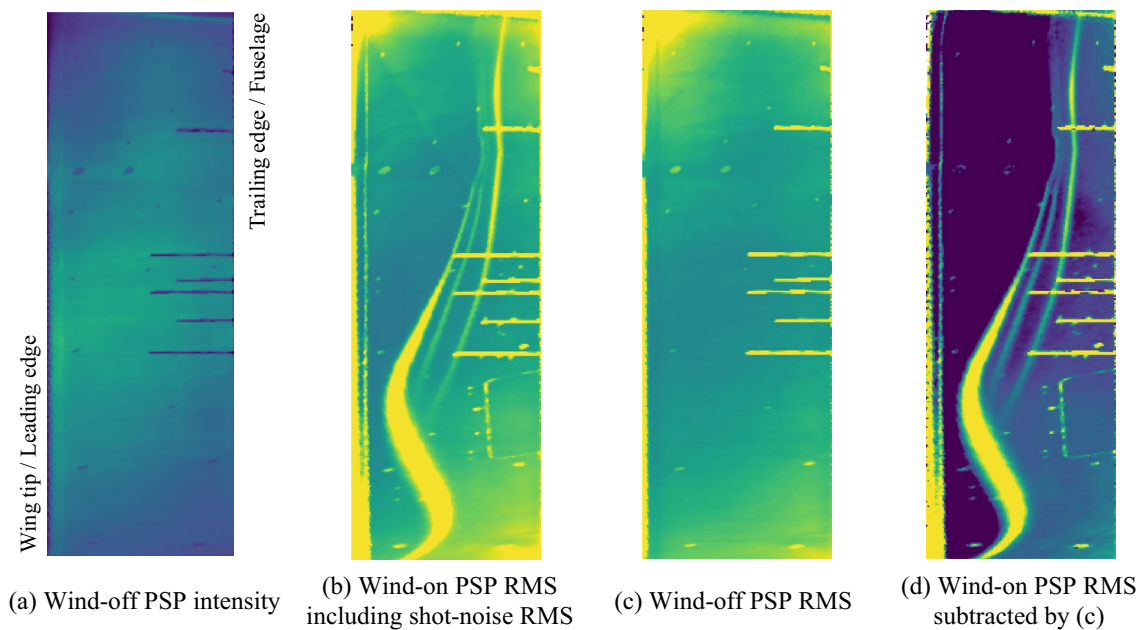
(a) Wind-off PSP intensity  (b) Wind-on PSP RMS including shot-noise RMS  (c) Wind-off PSP RMS  (d) Wind-on PSP RMS subtracted by (c)

**Fig. 13** Shot-noise RMS subtraction from the PSP RMS data using the wind-off PSP data

behind the shock. Our approach enables better quantitative RMS analysis from the unsteady PSP data.

**Data availability** The experimental data on the XRF1 configuration is not freely available. Data can be made available on request from two years after the respective measurement campaign has been carried out, provided that a valid XRF1 NDA with Airbus has been concluded by the recipient of the test data.

## References

1. Liu, T., Sullivan, J.P., Asai, K., Klein, C., Egami, Y.: Pressure and temperature sensitive paints, 2nd edn. Springer, Cham (2021). https://doi.org/10.1007/978-3-030-68056-5
2. Gregory, J.W., Sakaue, H., Liu, T., Sullivan, J.P.: Fast pressure-sensitive paint for flow and acoustic diagnostics. Annu. Rev. Fluid Mech. **46**, 303–330 (2014). https://doi.org/10.1146/annurev-fluid-010313-141304
3. Sugioka, Y., Koike, S., Nakakita, K., Numata, D., Nonomura, T., Asai, K.: Experimental analysis of transonic buffet on a 3D swept wing using fast-response pressure-sensitive paint. Exp. Fluids (2018). https://doi.org/10.1007/s00348-018-2565-5
4. Gößling, J., Ahlefeldt, T., Hilfer, M.: Experimental validation of unsteady pressure-sensitive paint for acoustic applications. Exp. Therm. Fluid Sci. (2020). https://doi.org/10.1016/j.expthermflusci.2019.10991
5. Quest, J.: ETW—High quality test performance in cryogenic environment. In: 21st AIAA Aerodynamic Measurement Technology and Ground Testing Conference, (2000) https://doi.org/10.2514/6.2000-2206
6. Yorita, D., Klein, C., Henne, U., Ondrus, V., Beifuss, U., Hensch, A., Guntermann, P., Quest, J.: Application of lifetime-based pressure-sensitive paint technique to cryogenic wind tunnel test. In: 54th AIAA Aerospace Sciences Meeting, (2016) https://doi.org/10.2514/6.2016-0649
7. Yorita, D., Klein, C., Henne, U., Ondrus, V., Beifuss, U., Hensch, A., Guntermann, P., Quest, J.: Investigation of a pressure sensitive paint technique for ETW (Invited). In: 55th AIAA Aerospace Sciences Meeting, (2017) https://doi.org/10.2514/6.2017-0335
8. Yorita, D., Klein, C., Henne, U., Ondrus, V., Beifuss, U., Hensch, A., Longo, R., Guntermann, P., Quest, J.: Successful application of cryogenic pressure sensitive paint technique at ETW. In: 2018

AIAA Aerospace Sciences Meeting, (2018) https://doi.org/10.2514/6.2018-1136

9. Lutz, T., Kleinert, J., Waldmann, A., Koop, L., Yorita, D., Dietz, G., Schulz, M.: Research initiative for numerical and experimental studies on high speed stall of civil aircraft. J. Aircr. (2022). https://doi.org/10.2514/1.C036829

10. Mann, A., Thompson, G., White, P.: Civil aircraft wind tunnel feature rich testing at the edge of the envelope. In: Proceedings of the 54th 3AF International Conference on Applied Aerodynamics (2019)

11. Yorita, D., Henne, U., Klein, C.: Improvement of lifetime-based PSP technique for industrial wind tunnel tests. In: 55th AIAA Aerospace Sciences Meeting, (2017) https://doi.org/10.2514/6.2017-0703

12. Nakakita, K.: Unsteady pressure distribution measurement around 2D-cylinders using pressure-sensitive paint. In: 25th AIAA Applied Aerodynamics Conference, (2012) https://doi.org/10.2514/6.2007-3819

13. Puklin, E., Carlson, B., Gouin, S., Costin, C., Green, E., Ponomarev, S., Tanji, H., Goutermann, M.: Ideality of Pressure-Sensitive Paint. I. Pl atinum tetra(pentafluorophenyl)porphine in fluo- reacrylic polymer. J. Appl. Polym. Sci. **77**(13), 2795–2804 (2000). https://doi.org/10.1002/1097-4628(20000923)77:13%3c2795::AID-APP1%3e3.0.CO;2-K

14. Masuda, T., Isobe, E., Higashimura, T.: Poly[1-(trimethylsilyl)-1-propyne]: a new polymer synthesized with transition-metal catalysts and characterized by extremely high gas permeability. J. Am. Chem. Soc. **105**(25), 7473–7474 (1983). https://doi.org/10.1021/ja00363a061

15. Klein, C.: Time resolved pressure measurements by means of PSP in cryogenic conditions. In: AIAA SCITECH 2022 Forum, (2022) https://doi.org/10.2514/6.2022-1938

16. Pastuhoff, M., Yorita, D., Asai, K., Alfredsson, P.: Enhancing the signal-to-noise ratio of pressure sensitive paint data by singular value decomposition. Meas. Sci. Technol. (2013). https://doi.org/10.1088/0957-0233/24/7/075301

17. Ali, M.Y., Pandey, A., Gregory, J.W.: Dynamic mode decomposition of fast pressure sensitive paint data. Sensors **16**(6), 862 (2016). https://doi.org/10.3390/s16060862

18. Weiss, A., Geisler, R., Schwermer, T., Yorita, D., Henne, U., Klein, C., Raffel, M.: Single-shot pressure-sensitive paint lifetime measurements on fast rotating blades using an optimized double shutter technique. Exp. Fluids (2017). https://doi.org/10.1007/s00348-017-2400-4